

Preliminary Design Review

Submitted in partial fulfillment of the requirements for

ENGS 89: Engineering Design Methodology and Project Initiation

Drone Object Sensing with Light Angle Sensor

November 10th, 2017

Sponsored by

Analog Devices, Inc.

Project Team #6

Hamza Alsarhan, Martin Anguita, Lotanna Ezenwa, Ping-Jung Liu, Prescott McLaughlin,
Arun Reddy

Faculty Adviser

Dr. Minh Q. Phan



Executive Summary

Analog Devices, Inc. (ADI) has developed a new optical sensor capable of measuring the three-dimensional angle to an infrared (IR) light source. ADI seeks to showcase the capabilities of their novel technology in a robotics application in order to appeal to their target market. Therefore, ADI has requested that the sensor be integrated within the navigation system of a quadcopter drone, allowing it to track and follow an IR light source.

ADI currently has evaluation boards that demo the sensor in a limited capacity due to the synchronous implementation of the sensor and light source. For this reason, the current evaluation boards would not be applicable in the inherently asynchronous drone-based demonstration. Our team is tasked with addressing the company's need for an engaging demonstration platform, as well as the asynchronous system capabilities needed to implement it.

The overarching goal for this project is to provide ADI with a reliable and engaging demonstration that showcases the distinguishing features of the sensor. Accomplishing this relies upon development of an asynchronous sensor system and its incorporation into the autonomous navigation of a drone. Figure 1 offers a system overview of the component integration required to achieve this.

At the onset of the term we recognized that the problem could be initially approached by independently developing the drone and sensor systems. Over the course of ENGS 89 we have successfully implemented the LED driving circuitry, the analog front end circuitry, and developed the signal processing necessary to reliably compute X and Y measurements. We have also succeeded in controlling the drone's actuators using an external input to the flight controller. Next steps toward project completion involve resolving the third spatial coordinate and incorporating the measurements into a robust control scheme.

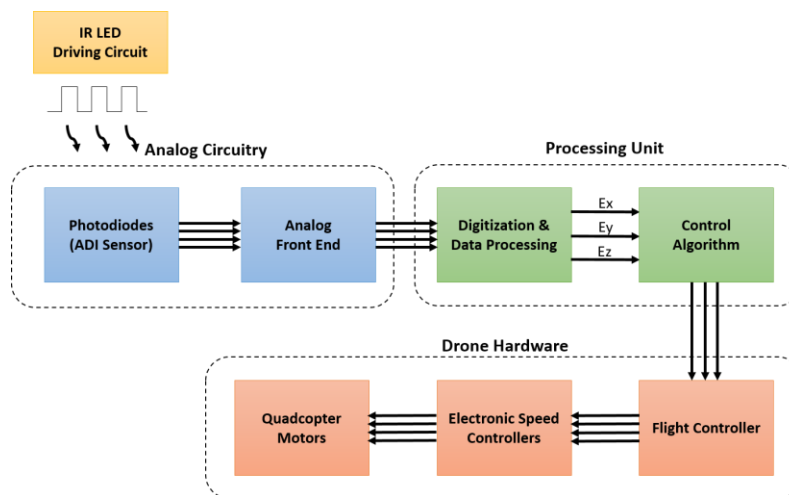


Figure 1. System overview of sensor implementation flow

Table of Contents

Executive Summary	i
Table of Contents	ii
List of Abbreviations & Acronyms.....	iv
1. Introduction.....	1
2. Problem Statement.....	1
3. Objectives and Requirements	1
4. Deliverables	2
5. Requirement Specifications.....	2
6. Previous Concerns	3
7. Research.....	4
7.1 Object Tracking	5
7.2 Control Algorithms for Object Tracking.....	5
8. Trade Studies and Engineering Analysis	5
8.1 Depth Measurement Method	6
8.2 Modulated Signal Detection Algorithm	7
8.3 Control Algorithm Selection & Implementation.....	8
9. Design Development.....	9
9.1 LED Driving Circuit Design.....	10
9.2 Sampling & Demodulation	10
9.3 Data Collection & Analysis	11
10. Risks and Mitigation Plans.....	13
11. Economic and Cost Analysis	14
11.1 Market Analysis	14
11.2 Cost.....	14
12. Client and Consultant Interaction.....	14
13. Project Management.....	15
References.....	16
Appendix A: Drone Characterization and Eye Safety.....	18
Appendix B: Function Tree.....	21

Appendix C: Light Source Modulation Scheme.....	22
Appendix D: Processing Unit Selection.....	24
Appendix E: Flight Controller Selection	26
Appendix F: Analog Front End Design.....	27
Appendix G: PCB Design.....	31
Appendix H: Benchtop Test Setup	33
Appendix I: Teensy Code	34
Appendix J: Histogram of Acquired Data.....	37
Appendix K: Total Costs	38
Appendix L: Future Plans.....	39
Appendix M: Revised Client Agreement	40

List of Abbreviations & Acronyms

ADC	Analog-to-Digital Converter
ADI	Analog Devices, Inc.
AFE	Analog Front End
BPF	Band Pass Filter
BW	Bandwidth
FFT	Fast Fourier Transform
DFT	Discrete Fourier Transform
DSP	Digital Signal Processing
IIR	Infinite Impulse Response
SPS	Samples per Second
FPGA	Field Programmable Gate Array
HF	High Frequency
IR	Infrared
IREM	Infrared Emitting Diode
LAS	Light Angle Sensor
MCU	Microcontroller Unit
PCB	Printed Circuit Board
PD	Photodiode
PID	Proportional plus Integral plus Derivative
SMD	Surface-mount Device
SNR	Signal-to-Noise Ratio
SOA	State-of-the-Art

1. Introduction

Analog Devices, Inc. is an industry leader in the design, manufacture, and marketing of a wide array of integrated circuits (ICs). Within its line of optical sensing products, the company has developed a novel device called a “light angle sensor.” The sensor is capable of discerning the X and Y coordinates of an infrared light source.

ADI is now seeking a way to showcase the impressive features of the sensor. Since a demonstration can add significant value to a product, the company has decided to invest some resources into developing a compelling demonstration. Recognizing that the sensor would be useful in robotics applications, ADI has elected a drone-based demonstration platform. Specifically, using the sensor for object tracking and following would provide an effective and exciting means of displaying the sensor’s features.

2. Problem Statement

ADI has developed demo boards that show the effectiveness of their sensor in some applications. These applications, however, rely on an on-board, synchronous light source. Since a drone object-following demonstration is an inherently asynchronous application, the company’s current platforms would not be effective in this case (namely due to insufficient sampling rate).

Therefore, the client’s problem is twofold: ADI lacks an engaging demonstration platform for their light angle sensor, as well as the asynchronous system capabilities needed to implement it.

3. Objectives and Requirements

Our team has worked with the sponsor, faculty, and technical advisors to identify the characteristics that make up a successful drone-based demonstration of the light angle sensor. Each member of the group independently ranked the requirements on a scale of 1-5 (5 being most important) with equal weight applied to each submission. The ranking revealed that the requirements should primarily focus on function, as this demonstration has inherent means and constraints that are more fitting as requirement specifications. The top 5 ranked requirements have been clarified in terms of functionalities.

Reliable Following: The drone being navigated by the sensor should follow its source with an adequate response to stay within the FOV of the sensor’s capabilities. This will be determined by the dynamic range we accomplish as gains and output power of IR source solidify.

Emergency Protocol: To build redundancy into the system, safety precautions need to be in place should the drone get outside of the FOV of the sensor and lose the ability to autonomously navigate. This should include a way to regain control of the drone so it is not flying blind.

3-D Tracking: To showcase the full scope of the sensor’s capabilities the demo must provide a clear indication of 3-D signal recognition. For the drone this means that it must be able to move in all 3 coordinate system and respond to the light sources shift across any combination of these.

Eye Safety: The demo must function as expected without posing any danger to the eye safety of viewers in terms of IR light exposure limits.

Captivate Consumers: Although this requirement is crucial, it is difficult to quantify it since it is not numerical. The best way to determine success is to ensure that the sponsor is satisfied that the demo and its illustration of the outlined distinguishing factors of the sensor.

Table 1. Objectives and Requirements

Category	Objective	Requirements	Metric	Rank
Function	Safety	Reliable Following	Stays within sensor FOV	4.7
		Avoid eye damage	IR Output < safe limit	4.2
		Emergency protocol	Maintain control outside FOV	4.7
	Demo showcases features of LAS	Capable of dynamic tracking	Track object with varying speed	3.3
		Capable of 3-dimensional tracking	Track object in X, Y, Z	4.3
		Minimal complexity	Less complex than CMOS camera-based system	3.7
	Captivating demo	Draws interest of demo viewers	Meets sponsor expectation	3.8
	Replicable	Does not require extensive training	Application engineer can show demo independently	3.0
	Easy implementation	Does not require extensive setup	Ready in < 5 mins	3.2
	Conveys Meaning	Effectively convey to consumer the purpose of the demo	Requires < 1 min. to explain	3.7
Means	Power Availability	Sufficient onboard power for demo	Demo > 10 min/charge	3.3
Constraints	Operate using existing follower drone	Adheres to physical limitations of follower drone	Source moves within reaction parameters	2.7

4. Deliverables

- A printed circuit board (PCB) that incorporates the light angle sensor, analog front-end circuitry and digital signal processing necessary to measure X, Y, and Z position of an asynchronous light source
- A PCB that implements a square-wave LED driving circuit which will serve as the IR light source in the demonstration
- A functioning demonstration that showcases the operability of the light angle sensor in a drone-based object-following application
- Appropriate documentation of hardware and software implementation details

5. Requirement Specifications

With a successful demonstration outlined above, the overarching system can be broken into four sub-categories that make up the solution space. Requirement specifications have been

determined for each of these sub-systems through comprehensive planning of the system integration as well as the functionality needed in each component. Table 2 outlines these specifications and their inherent contribution to fulfilling the objectives and requirements seen in Table 1.

Table 2. Requirement Specifications

Sub-System	Requirement Specification
Sensor	Maximize SNR
	Provide adequate BW for control algorithm
	Discern spatial changes within 1.5 m Z-offset
	Function using 5 V or 3.3 V onboard power
	Sample fast enough to avoid aliasing ($10\times$ LED frequency)
	Reliably detect spectral content at LED frequency (500 Hz)
LED Source	Reliable production of 50% duty cycle & 500 Hz frequency
	Minimal power consumption for low power application on toy drone
	Able to produce maximum safe output power (up to 570 mW/m ²)
	Safe for demo: i.e. adheres to eye safety standards
	Frequency separated from ambient noise ($\gg 120$ Hz)
Controller/Processing Unit	Frequency low enough to be sampled by MCU ADC ($< f_{\text{sample}}/10$)
	Compatible with flight controller inputs
	Adequate BW for smooth autonomous control (> 10 Hz at output)
Drone/Flight Controller	Intuitive transient response tuning for testing
	Capable of stable flight (Can reliably align prior to autonomous state)
	Compatible with external control input
	Can fly with payload up to 1 lb.

It is worth mentioning that there is a significant degree of co-dependence between sub-systems which results in some redundancy in requirement specifications across the components.

6. Previous Concerns

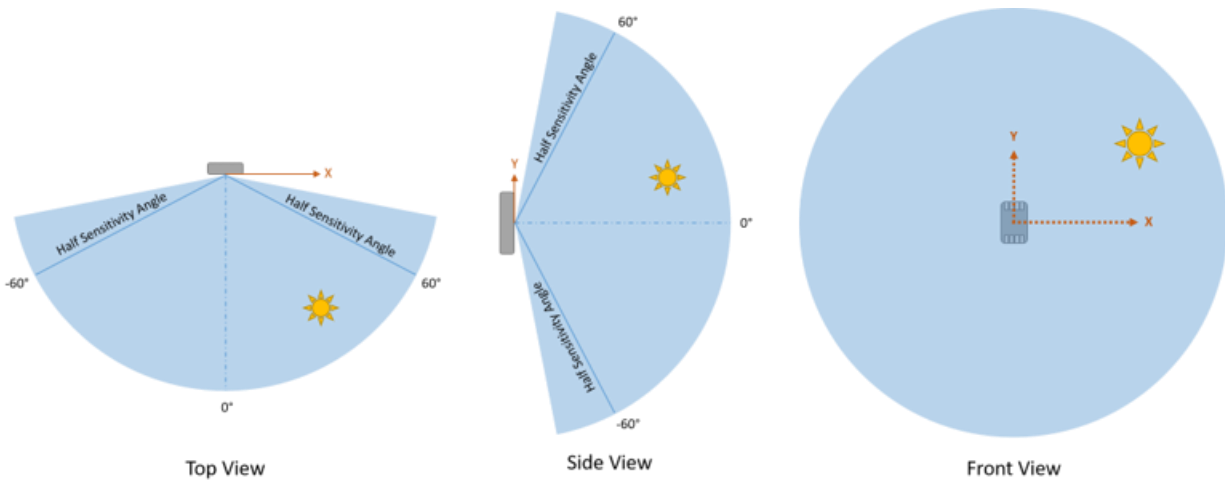


Figure 2. Functional Illustration of Sensor Operation

A few of the main suggestions made by the review board and course directors were: clarifying the scope of the project, providing a functional description of the LAS, and including more details of the demonstration itself. Thus, we begin with an overview of the sensor's functionality.

The LAS can discern the relative angle of incident light in the 2-D X-Y plane indicated in Figure 2. This is accomplished using four PDs, with peak responsivity at 850 nm that produce photocurrents proportional to the number of photons incident to each PD. With these relative signal intensities, the X and Y coordinate of the source relative to the sensors 2-D view plane can be produced using the equations seen in Figure 3.

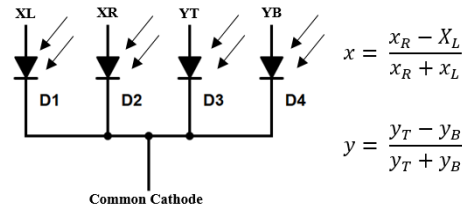


Figure 3. Schematic Representation of PD functionality to produce relative coordinates

The sensor is an entirely passive component that produces photocurrents on the order of micro-amps (μA) that must then be converted into voltages of a magnitude that can be effectively sampled, processed, and incorporated into the control system of the drone. It is in these processes that power consumption occurs. Given that these coordinates are within a 2-D plane, there must also be a methodology to discern distance to the object, which will be discussed in Section 8.1.

Another aspect of the project to consider is the demonstration, as it must illustrate the features of the LAS that distinguish it from competitors in the optical sensor space. The demonstration will involve attaching the IR light source to an object that the drone will follow, maintaining a specified distance and angle. We plan to systematically develop it in complexity to verify functionality as we move toward the conclusion of ENGS 90.

The overarching concern that we have been addressing throughout ENGS 89 is the scope of our project and what it entails to accomplish an object-following demonstration. We have thus tailored our requirements to focus on the achievement of a successful demonstration, which we believe has clarified the scope of the project.

7. Research

The most relevant research topics: object tracking and control algorithms, have been outlined below. The findings indicate a prevalent use of cameras for object recognition, combined with PID compensators to adjust the positioning of the quadcopter. Subjects such as eye safety guidelines and quadcopter characterization are reported in Appendix A.

7.1 Object Tracking

Current technologies employed for navigation include ultrasonic sensors, infrared sensors, visible light cameras, and infrared cameras. More specifically, the current methods of tracking a moving object are limited to using cameras. One example of how a camera can be used to track an object is presented by Kendall et al [10], where a quadcopter is outfitted with a camera and designed to track a round orange object. Their controller calculates the position of the drone with respect to the ball by measuring the amount of pixels between the center of the screen to the ball. Meanwhile for distance, the diameter of the ball on the image is used. These measurements are then used to generate a control signal through the implementation of three PID controllers for yaw, height, and range. A graphic representation of this can be seen in Figure 4.

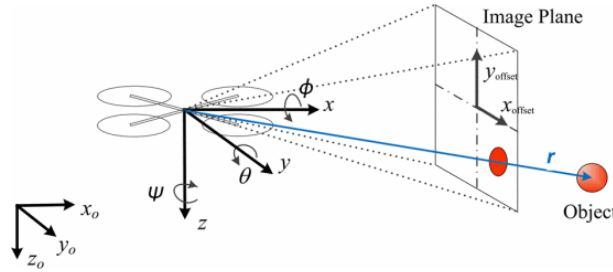


Figure 4. 3-D representation of quadcopter coordinates from Kendall et al.

7.2 Control Algorithms for Object Tracking

PID controllers are the most popular method for controlling the stability of a quadcopter, along with its positioning with respect to a tracking object. Some publications make use of proportional-derivative controllers such as Pestana et al [16]. For drones that make use of video sensing technology, many tracking algorithms exist, one of which is called the Lucas-Kanade algorithm [4] which estimates motion between two subsequent pictures from its onboard video feed in order to predict the motion of the object to be tracked.

There are examples of more unique control algorithms employed by some research groups, such as a fuzzy logic controller implemented by Algabri et al [2]. This algorithm mimics the behavior of a human closer than a PID or state feedback controller would. Replicating a user input will generate a controller of basic performance that will suffice. An approach similar to that of the fuzzy logic controller could be employed in our application, utilizing the inherent stability controls in the flight controller, providing only heading commands to the quadcopter through the sensor's positioning control algorithm.

8. Trade Studies and Engineering Analysis

Since the high-level structure of the required system is well-understood, our trade studies focus on the design decisions involved in developing some of the individual blocks in the system. Given the large number of sub-components involved in the overarching system we list the top three representative trade studies below with some remaining decision-making processes

included in Appendix C, D and E. A function-means tree illustrating design choices and implications can be found in Appendix B.

8.1 Depth Measurement Method

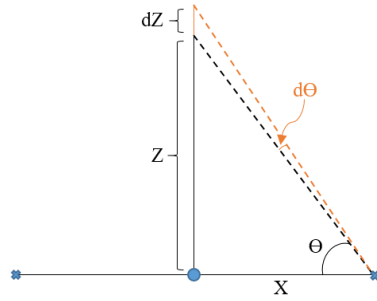


Figure 5. Triangulation Calculation Diagram

Our ultimate goal in this project, which is to enable a quadcopter to track and follow a light source in three-dimensional space, requires that our sensing apparatus is able to accurately measure the distance to the source. While the LAS's outputs provide X and Y coordinates, it does not provide a direct way of measuring the third spatial coordinate (distance). We have identified two potential methods to determine the third spatial dimension of the light source with respect to the sensor. The first relies on an accurate model of intensity to determine distance to the light source. The second uses two sensors placed a fixed distance apart to triangulate the Z location of the source using the X and Y angles provided by the sensor's 2-D functionality.

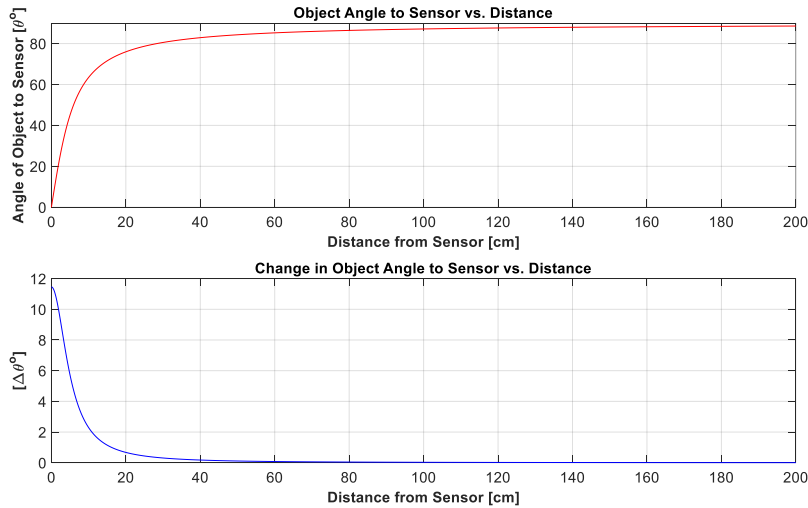


Figure 6. Angular dependencies as a function of distance

Triangulation is the approach currently utilized by ADI in their demo boards and with this, we began by evaluating its feasibility for a longer range solution. We chose a maximum sensor separation of 10 cm that could be implemented on a PCB, with X in Figure 5 representing 5 cm. The top of Figure 6 shows the effect of sweeping Z from 0 to 2 meters on the angle seen by the

sensor. In addition we evaluated $d\Theta/dZ$ to illustrate how angular resolution falls off as a function of distance. This suggests that discerning angular changes will be difficult at the distances we will be operating in, as there are small angle deltas for large spatial gaps in distance. (Figure 6 bottom)

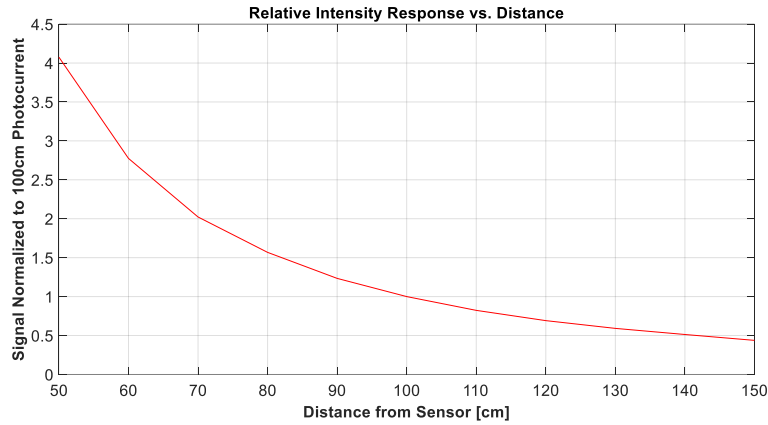


Figure 7. Sensor Photocurrent response as a function of distance

Our sponsors at ADI followed this by carrying out a relative sensor photocurrent characterization as a function of distance. The plot in Figure 7 indicates promise for this method, as it is clear that the signal is definitively capturing distance changes out to 150 cm.

8.2 Modulated Signal Detection Algorithm

Once the modulated IR signal from the light source reaches the sensor system, it must be digitally demodulated to perform the spatial measurements. In our case, this demodulation process is rather simple and amounts to recognizing the magnitude of the 500 Hz content on each of the four photodiode channels. We compared a few demodulation methods and chose the best alternative.

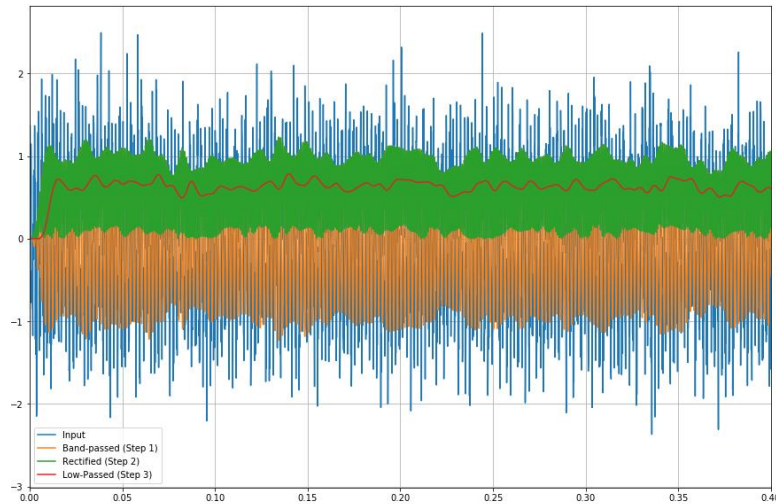


Figure 8. 3-stage demodulation scheme using BPF, rectifier, LPF

The first option considered is most intuitive in the time-domain. It essentially consists of applying a tight band-pass filter around the modulation frequency, rectifying the result, and determining the envelope of the rectified signal with a low-pass filter. Figure 9 shows a simulation of how this method would demodulate a varying 500Hz signal.

While this process seems simple, the tight band-pass filter and final low-pass filter are computationally taxing since they require hundreds of multiplications with digital filter taps. Since these computations will be performed on a processing unit that is also performing other functions, it is in our best interest to minimize computation time and maximize bandwidth.

Another option is to perform an FFT and look for the magnitude of the modulation frequency. For our application, computing only a few FFT bins would be sufficient, since the rest of the spectral content is of little interest to us. When computing individual terms of a DFT, a DSP technique called the Goertzel algorithm is computationally advantageous over the FFT [5]. When computing M points of the DFT from N data points, the complexity of the two methods are:

$$FFT: \quad O(KN \log N)$$

$$Goertzel \text{ Algorithm: } O(KNM)$$

As long as the number of DFT bins needed is less than $\log(N)$, which is true in our case, the Goertzel algorithm proves less computationally complex than the FFT. For this reason, the Goertzel algorithm was chosen as the demodulation method. A more detailed description of the algorithm's implementation is given in section 9.2.

8.3 Control Algorithm Selection & Implementation

After thorough research of the control algorithms being implemented in both research applications and available drones for sale, it is clear that the PID controller is the most commonly used one. In most cases where a drone is made to follow and track an object, these controllers not only compensate for the position of the quadcopter with respect to the object, but are also used to stabilize the drone's flight.

In the case of the project at hand, the ultimate goal dictates that the drone simply follow the light source, and therefore the scope of the project focuses solely on the commands given by the error in spatial positioning with respect to the IRED light beacon.

With this in mind, it was decided that the drone will be implemented with a flight controller (FC) which includes its own flight stabilization algorithms. Commands given to the FC will therefore simply mimic the inputs that a person would give a drone from a hand held transmitter. Allowing the drone to stabilize itself independently of the positioning controller affords us the flexibility to implement a very simple controller to compensate solely for the drone's positioning. An added advantage is the possibility of switching flight modes from *manual*, where a pilot will control the drone, to *tracking*, where the drone will follow the light source.

Having the option to switch back and forth between flight modes adds redundancy and safety, which are crucial for a demonstration. In the case that the control algorithm behaves erratically, the user can simply switch to manual flight in order to avert disaster.

The positioning algorithm will therefore be implemented on a separate microcontroller, which will command the FC to either climb in height, translate sideways (roll), or move back and forth (pitch). The commands given to the FC must therefore replicate those provided by the radio transmitter. One approach we analyzed for communicating with the FC was through an I²C bus, yet we rejected it due to the complexity involved and the alterations required to the FC firmware. Currently, we have implemented a potentiometer to mimic the output of the positioning algorithm, proving that an external signal can provide valid commands for the FC.

The positioning control algorithm will take the form of a proportional controller, with independent gains for each of the three translations in 3-dimensional space. Doing so will provide the ability to tune each translation separately, thus, allowing to improve the efficiency of each translation.

$$\hat{U} = K_p \cdot \hat{e} \quad \text{Where } \hat{U} = \begin{bmatrix} u_x \\ u_y \\ u_z \end{bmatrix}, \hat{e} = \begin{bmatrix} e_x \\ e_y \\ e_z \end{bmatrix}, \& K_p = \begin{bmatrix} k_x \\ k_y \\ k_z \end{bmatrix} \quad (1)$$

Equation 1 represents the proportional controller, with input vector \hat{U} feeding to the Parallax, being the result of multiplying the position errors \hat{e} by gain vector K_p , which will be tuned through an iterative experimental process. The overall compensator design can be seen in figure 10.

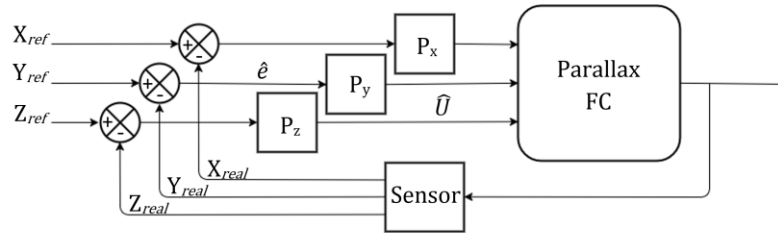


Figure 9. Positioning controller breakdown, illustrating the use of three separate proportional controllers to regulate the width of the ‘high’ signal to the Parallax FC.

For the winter term, we will analyze the potential to use a PID controller. Yet, for first round testing, we will implement a proportional controller with extremely conservative gains.

9. Design Development

Our overall design philosophy is to provide enough room for each component to work, then optimize it following validation. With this, design of each component below is outlined and shows its contribution to the progress of the overarching system. Each module is designed in

accordance with the requirement specifications listed in Section 5 to achieve success of the combined system. The development of the LED driving circuitry, the demodulation scheme, and the data collection process are described here, while details regarding AFE circuitry and PCB design can be found in appendix F and G respectively.

9.1 LED Driving Circuit Design

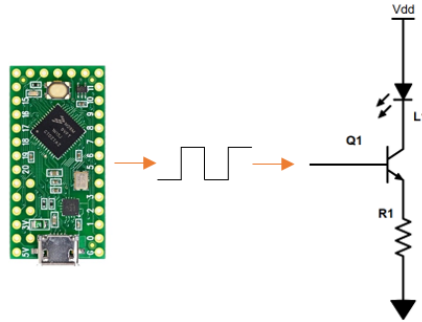


Figure 10. Schematic representation of LED driving circuit

The LED driving circuit functions by utilizing the square wave generated by the MCU to drive a switch. Toggling the switch in this way allows current to flow through the LED as a square wave. The emitter resistor sets the current that flows through the LED when the switch is closed, thus controlling our emission power.

This current was chosen bearing in mind the power needed to operate at our following distance based on the sensor's response characterization. With this, output power needed is correlated to a given current using the relative total radiant flux provided on the datasheet for the OSRAM SFH 4716AS to determine the current needed. [14]

This LED was chosen for its output wavelength of 850 nm, which is the wavelength for which the LAS achieves peak responsivity. In addition, the LED chosen has a wide angle (150°), which is important because it makes for a uniform distribution of its output that does not require strict considerations of its angle of irradiance for our receiving side.

The circuit must be designed to function on low power while maximized for efficiency, as it will eventually be mounted on a low power platform. With this in mind, the voltage V_{dd} must be at a minimum that includes the forward voltage of the LED at our driving current, the voltage drop across the switch, and the voltage drop across the resistor. There should be a small excess of potential to ensure that when the square wave is at its peak there is enough potential to source the current necessary to output our desired peak IR output intensity.

9.2 Sampling & Demodulation

After the AFE, the sensor signal is ready to be sampled by the microcontroller and processed to produce X and Y measurements. The speed of Arduino's built-in "analogRead()" function was first analyzed to determine whether a custom function would need to be written in Assembly. The function was found to take close to 20 microseconds to complete. This corresponds to a

maximum sampling rate of 50 kSPS, or 12.5kSPS per channel. This is much lower than the sampling rate indicated on the Teensy 3.5 datasheet due to the overhead associated with the Arduino programming language. However, since our frequency of interest is 500Hz, the sampling rate possible with `analogRead()` is sufficient for at least 20x oversampling. Thus, 10 kSPS was chosen as the sampling rate for each channel.

The microcontroller needs to both sample the incoming analog signals as well as process the generated data. Since the Goertzel algorithm can be implemented in the form of an IIR filter, it can either act on a continuous stream of data or on a buffer of many data points. Buffering a set of data, then operating on it all at once, is more computationally efficient than a streaming approach [19]. Thus, an interrupt service routine (ISR) was implemented for precise sampling, and the data processing was performed on a buffer of data in the main loop of the program. After the data buffer is filled by the sampling ISR, interrupts are disabled, the computations are performed, and interrupts are re-enabled so that the next data buffer can be filled. A buffer size of 200 samples was chosen, since this would capture 10 periods of our modulated signal. A larger buffer of data would improve the accuracy of the Goertzel algorithm, but would decrease the update rate of our X, Y, and Z measurements. In our case, buffering 200 samples at 10 kSPS leads to an output update rate of 50 Hz. Looking at similar applications, we believe this update rate will be sufficient as an input to the eventual control algorithm.

After performing the Goertzel algorithm, the magnitude of 500Hz content seen by each of the four photodiodes is used to calculate the X and Y spatial coordinates of the light source. The microcontroller code can be found in appendix I.

Once an accurate intensity model is developed, the aggregate response of the four photodiodes will be used to determine the third spatial coordinate. An important consideration going forward will be to evaluate the effect of computing more than one DFT bin on the SNR of output measurements.

9.3 Data Collection & Analysis

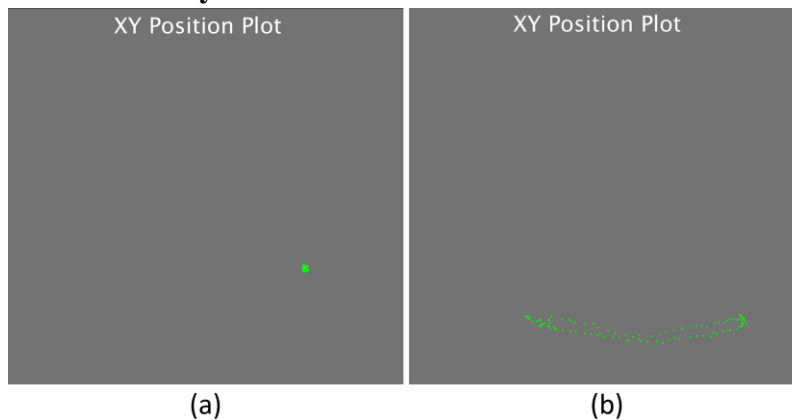


Figure 11. XY Measurement Plot (a) Stationary light source (b) Moving light source in X direction

Images of our benchtop test setup can be found in appendix H. The setup includes the IR light source, the sensor system, and allows data acquisition with connection to a PC. Figure 12 shows plots of X and Y measurements obtained from the microcontroller; it has a persistence of 100 samples to capture movement.

Figure 12(a) shows data obtained from a stationary light source located at a distance of 0.3 meters and an arbitrary angle from the sensor. Figure 12(b) shows data obtained while waving the light source back and forth in the X direction by a few centimeters. Since the data do not currently have physical meaning, axes are not included. However, the size of the cluster in (a) relative to the change induced by movement of the light source gives some idea of our SNR, suggesting we are able to reliably track changes of a few centimeters at a 0.3m distance with our current gain and IR intensity. In these tests, the current applied through our LED is $90\text{mA}_{\text{peak}}$ (45mA_{avg}), which is much lower than the possible safe current that could be applied. Increased light intensity will lead to higher SNR and an ability to track at farther distances. Appendix J shows more rigorous analysis of a similar situation.

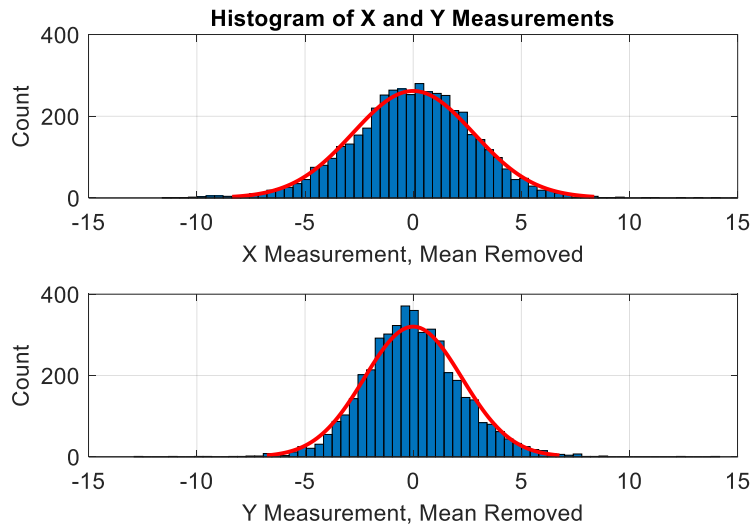


Figure 12. Depiction of Gaussian noise distribution for X and Y measurements

Figure 13 presents histograms of the X and Y measurements with mean removed to analyze the noise distributions. It indicates that both X and Y measurements contain noise with a roughly Gaussian distribution. It is also worth noting that the variance of the two distributions are roughly equal, suggesting minimal noise skew across axes.

To analyze the spectral content of the noise in the X and Y measurements, we performed an FFT on the data and the results are shown in figure 14.

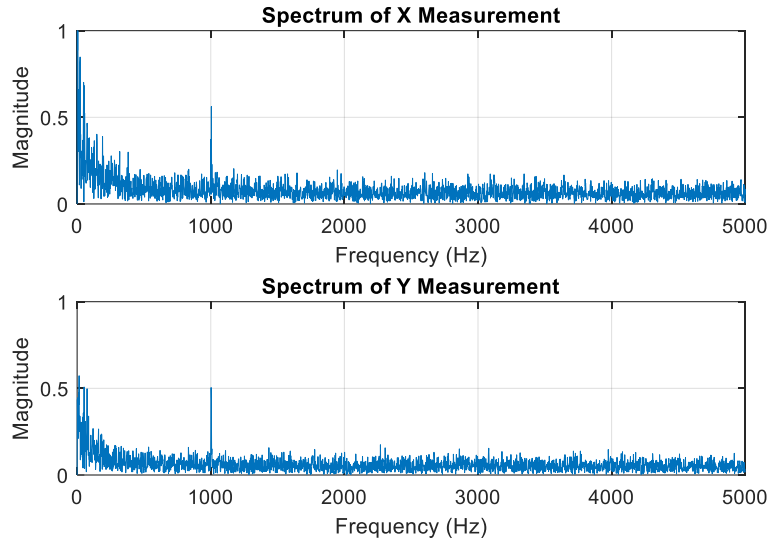


Figure 13. Noise Spectra of X and Y Measurements

The noise in both the X and Y measurements were found to have very significant spectral content at 1kHz. The source of this noise is currently unknown and will be studied further. Regardless of the source, the 1kHz noise can be easily removed by implementing a simple (moving average) filter on the microcontroller.

The results presented here make a compelling case for the feasibility of this sensor system in discerning the X and Y coordinates of a light source, especially since we now know that the intensity of the source can be increased considerably without inflicting eye damage.

10. Risks and Mitigation Plans

The first major pitfall encountered was the non-flying drone provided by ADI. When we found that the problem was that the provided FC was unable to calibrate, we purchased a new FC. The Parallax FC was acquired due to its suitability for the project. It can be programmed with an IDE designed by the company, which eases use.

The second challenge involved the communication from the positioning controller to the FC. Finding a solution involved analyzing the options of using either I²C or the RC input channels. Since this was established as an important milestone at the beginning of ENGS 89, the team focused two weeks to making sure an external source could control the motors through the FC.

Risks that could affect future success of the project include the difficulty in setting the correct PID gains in the FC, and the transition from manual to automatic flight modes. Picking these will determine the flight stability of the drone, and they must be done experimentally through the GUI provided by Parallax, Inc. In order to provide a steady transition from manual to automatic modes, an appropriate distance for initial positioning of the light source will have to be determined so as not to stimulate a large impulse response in the drone.

11. Economic and Cost Analysis

11.1 Market Analysis

As our client provides solutions for industries involving digital and analog systems, they plan to target automation in vehicles. The light angle sensor can be integrated into circuits involving microprocessors and controllers. Market research shows that consumer electronics is the broadest market that could make use of our light angle sensor, which would therefore be the total addressable market in the U.S. (TAM). Estimated TAM revenue was 224 Billion USD in 2016 [21]. The served addressable market (SAM) consists of the sensor market in the US, with an estimated revenue of 15 Billion USD [17].

The markets foreseen utilizing the sensor, our target market (TM), are the autonomous land and aerial vehicle markets. Furthermore, it is estimated that fully autonomous vehicles will be on the roads by 2022 [8]. Based on the growth of these markets, and assuming a \$20 cost for an entire sensor system and a conservative 10% market share, the total combined revenue for ADI could exceed 200 million USD [9].

The ultimate goal of ADI is to showcase this platform at trade shows, where clients of several different areas can appreciate the sensor's versatility. Moreover, ADI's Marketing Manager reaffirmed that although it is difficult to show correlation between the sales before and after a demonstration, there is a direct relationship between the quality of the demonstration and the increase in sales. Difficulties in quantifying this correlation stem from the fact that most demonstrations are function specific as per the request of a client and are usually produced as a collaboration between ADI and the client's engineering teams.

11.2 Cost

The Marketing Manager at ADI provided essential information on the pricing of the sensor, the market size, as well as the impact of demonstrations on sales. As it stands, a batch of 1000 light angle sensors similar to the one we have is sold at \$2.97/sensor. The combination of the sensor with an evaluation board sold by ADI would bring the total cost to approximately \$20. For a more detailed list of expenses, please refer to Appendix K.

12. Client and Consultant Interaction

Weekly conference calls and frequent email communication ensure that our sponsor is up-to-date on the progress of the project, allowing them to provide valuable input. Additionally, ADI has offered to cover additional costs if funds are depleted.

Thayer professor Jason Staath has assisted with the high-level validation of our AFE circuitry to effectively utilize the sensor's photocurrents and minimize noise. He also provided insight on the LED driving circuit and on how to achieve fixed current through an LED at square-wave peak, along with efficiency considerations. Most recently, he has helped us validate the layout of our PCB. Professor Kofi Odame has advised on the choice between sine-wave and square-wave to drive the LED, as well as ways to generate these waveforms. Professor Stephen Taylor has

helped in the choice of external vs. MCU ADC, for bandwidth specifications, and on the MCU interrupt protocols. Professor Minh Phan has provided instrumental guidance in directing us to a LUT-based proportional control algorithm.

13. Project Management

Now that we have achieved our goals for ENGS 89, we have developed an effective plan for completion of the entire project. For an outline of this plan please refer to Appendix L. Some of the major technical goals over the remaining weeks include discerning the third spatial coordinate, validating and revising the sensor PCB, designing and ordering the LED driving PCB, modeling and developing the control algorithm, and integrating all sub-systems.

To characterize the distance response of the sensor, we have acquired optical stages from Professor Levey that will be utilized for accurate measurement. For drone testing we will initially utilize the large frame lab initially with a contingency plan to gain permission for testing in the Leverone Field House should we require a larger space.

Over winter break we plan to stay in contact with each other to complete any MATLAB simulations needed for control algorithm development. In addition we will be optimizing circuit designs using LTSpice and Eagle from the Virtual Lab and detailing our plans for ENGS 90.

Division of labor will play a crucial role in the success of our project. Arun and Prescott will be responsible for the electronics design as well as the signal processing involved in making accurate spatial measurements. Marty and Lota will focus on development of the control algorithm that will convert the 3-D error signal into motor actions. Ping and Hamza will focus on implementation of the control algorithm as well as developing the capability to switch between manual control and autonomous object-following.

References

- [1] Achtelik, Markus, Tianguang Zhang, Kolja Kuhnlenz, and Martin Buss. "Visual Tracking and Control of a Quadcopter Using a Stereo Camera System and Inertial Sensors." *IEEE Xplore*, 18 Sept. 2009, doi:10.1109/ICMA.2009.5246421. Accessed 9 Nov. 2017.
- [2] Algabri, Mohammed, Hassan Mathkour, MOhammed A. Mekhtiche, Mohammed A. Bencherif, and Mansour Alsulaiman. "Wireless Vision-Based Fuzzy Controllers for Moving Object Tracking Using a Quadcopter." *International journal of Distributed Networks*, vol. 13, no. 4, 27 Apr. 2017. Accessed 9 Nov. 2017.
- [3] *Analog Devices*, 3 Oct. 2017, <https://wiki.analog.com/resources/eval/user-guides/eval-adicup360>. Accessed 9 Nov. 2017.
- [4] Bartak, Roman, and Adam Vyskovsky. "Any Object Tracking and Following by a Flying Drone." *IEEE Xplore*, 10 Mar. 2016, doi:10.1109/MICAI.2015.12. Accessed 9 Nov. 2017.
- [5] Evans, Brian L. "Goertzel Algorithm.", University of California, Berkeley, https://ptolemy.eecs.berkeley.edu/papers/96/dtmf_ict/www/node3.html. Accessed 9 Nov. 2017.
- [6] International Commision on Non-Ionizing Radiation Protection. *Guidelines on limits of exposure to incoherent visible and infrared radiation*, International Commision on Non-Ionizing Radiation Protection. , Health Physics, 2013, pp. 74-96, www.icnirp.org/cms/upload/publications/ICNIRPVisible_Infrared2013.pdf. Accessed 9 Nov. 2017
- [7] "EXCALIBUR LOW-NOISE HIGH-SPEED JFET-INPUT OPERATIONAL AMPLIFIERS." *www.ti.com*, Texas Instruments, Inc., Dec. 2009, www.ti.com/lit/ds/symlink/tle2072.pdf. Accessed 9 Nov. 2017.
- [8] "Forecasts." *Driverless car market watch*, 26 Oct. 2017, www.driverless-future.com/?page_id=384. Accessed 9 Nov. 2017.
- 3
- [9] Joshi, Divya. "Commercial Unmanned Aerial Vehicle (UAV) Market Analysis – Industry trends, companies and what you should know." *TECH INSIDER*, 8 Aug. 2017, www.businessinsider.com/commercial-uav-market-analysis-2017-8. Accessed 9 Nov. 2017.
- [10] Kendall, Alex G., Nishaad N. Salvapantula, and Karl A. Stol. "On-Board Object Tracking Control of a Quadcopter with Monocular Vision." *IEEE Xplore*, 26 June 2014, doi:10.1109/ICUAS.2014.6842280. Accessed 9 Nov. 2017.
- [11] "Kinetis K64F Sub-Family Data Sheet." *PJRC Electronics*, 8 June 2015, <https://www.pjrc.com/teensy/K64P144M120SF5.pdf>. Accessed 9 Nov. 2017.
- [12] Mondragon, Ivan F., Pascual Campy, Miguel A. Olivares-Mendez, and Carol Martinez. "3D Object Following Based on Visual Information for Unmanned Aerial Vehicles." *IEEE Xplore*, 28 Nov. 2011, doi: 10.1109/LARC.2011.6086794. Accessed 9 Nov. 2017.
- [13] Odame, Kofi M. "Compensating the Transimpedance Amplifier." Thayer School of Engineering at Dartmouth, Hanover, NH.

- [14] "OSLON Black Series (850 nm) - 150° Version 1.3 SFH 4716AS." *Viewpoint Systems*, OSRAM Opto Semiconductors GmbH , 1 Feb. 2012, www.osram-os.com/Graphics/XPic7/00204353_0.pdf. Accessed 29 Jan. 2016.
- [15] OSRAM. *Eye Safety IREDs used in lamp applications*, OSRAM. , OSRAM, 2010, www.osram-os.com/Graphics/XPic2/00052113_0.pdf/Application%20Note%20Eye%20Safety.pdf. Accessed 9 Nov. 2017.
- [16] Pestana, Jesus, Jose L. Sanchez-Lopez, Srikanth Saripalli, and Pascual Campoy. "Computer Vision Based General Object Following for GPS-denied Multirotor Unmanned Aerial Vehicles." *IEEE Xplore*, 21 July 2014, doi:10.1109/ACC.2014.6858831. Accessed 9 Nov. 2017.
- [17] "Sensors - Demand and Sales Forecasts, Market Share, Market Size, Market Leaders." , The Freedonia Group, Inc, Oct. 2012, <https://www.freedoniagroup.com/Sensors.html>. Accessed 9 Nov. 2017.
- [18] *STMicroelectronics*, 2016, www.st.com/en/evaluation-tools/nucleo-f401re.html. Accessed 9 Nov. 2017.
- [19] "Using Microcontrollers in Digital Signal Processing Applications." *www.silabs.com*, Silicon Laboratories, Inc., <https://www.silabs.com/documents/public/application-notes/an219.pdf>. Accessed 10 Nov. 2017.
- [20] *Viewpoint Systems*, <https://www.viewpointusa.com/industrial-embedded/when-is-an-fpga-worth-it-and-when-is-it-not-when-developing-an-industrial-embedded-system/>. Accessed 9 Nov. 2017.
- [21] Wholesale revenue consumer electronics (CE) shipments in the U.S. from 2009 to 2017 (in billions of U.S. dollars) <https://www.statista.com/statistics/272115/revenue-growth-ce-industry/>

Appendix A: Drone Characterization and Eye Safety

Quadcopter Characterization

Drone characterization involves a complicated nonlinear system of differential equations that is under-actuated as the plant can only be controlled through the thrust of four motors in order to stabilize its six degrees of freedom. These equations have to be linearized about a hover, which would provide an accurate approximation of the quadcopter's dynamics during small changes in roll and pitch angles.

Research showed that drone characterization was conducted in order to create efficient flight stabilization controllers, and not necessarily for the design of a position compensating algorithm. As was discussed in sections 7.1, 7.2, and 8.4, the current plan aims to avoid designing the stabilization control algorithms, and will focus on creating a positioning controller, which will navigate a drone being stabilized by the flight controller. Therefore, an accurate state space representation of the drone is not necessary if the aim is to mimic the commands given by a person flying the drone towards a target. An example application of this technique was presented by Mondragón et al, where the group successfully tracked a round orange object by simply providing the drone's flight controller with translation commands [12].

Eye Safety Concerns

Research into the hazards of using an infra-red light source as our tracking beacon was conducted in order to assess the limits of exposure. A report describing the calculations of these limits has been published by the International Commission on Non-Ionizing Radiation Protection (ICNIRP), in order to model general exposure scenarios to IR-A radiation ($\lambda = 780\text{-}1400\text{ nm}$) [6]. The manufacturer of the infrared emitting diode (IRED) being issued a guideline based on the ICNIRP's report, and both were used in conjunction to determine the health risk posed by the IRED. [15]

Damage to a person's eye can occur in either the retina or the cornea, and must therefore be analyzed separately. In order to determine the maximum allowed irradiance E_{IR} ($E_{e,\max}$), the following was used: [Grab your reader's attention with a great quote from the document or use this space to emphasize a key point. To place this text box anywhere on the page, just drag it.]

$$E_{IR} = \sum_{\lambda=780}^{3000} E_{\lambda} \cdot \Delta\lambda \leq \frac{18000}{t^{0.75}} \quad [W \cdot m^{-2}] \quad (2)$$

Where E_{λ} is the spectral irradiance in $W/m^2/nm$, $\Delta\lambda$ given in nm, and t is in seconds. Irradiance $E_{e,\max}$ can be calculated using the radiant intensity I_e that found in the datasheet for the IRED, and the distance d using the inverse square law:

$$E_e = \frac{I_e}{d^2} \quad [W \cdot m^{-2}] \quad (3)$$

Where d is in meters and I_e in W/sr.

Calculations for the radiance exposure limits for the iris were done with the following equation:

$$L_{IR} = \sum_{\lambda=780}^{1400} L_{\lambda} \cdot R(\lambda) \leq \frac{6000}{\alpha} \quad [W \cdot m^{-2} \cdot sr^{-1}] \quad (t > 10s) \quad (4)$$

Where L_{λ} is the spectral radiance in W/m²/nm/sr, α the angular subtense of the source in radians, and $R(\lambda) = 10^{(700-\lambda)/500}$ being the burn hazard weighting function. A very accurate approximation for L_{IR} , however can be obtained from the following equation in order to use datasheet values:

$$L_{IR} \approx \frac{I_e \cdot R(\lambda)}{((l + w)/2)^2} \quad [W \cdot m^{-2} \cdot sr^{-1}] \quad (5)$$

Where l and w are the length and width of the light source in meters.

Once all values were calculated, considering a forward current of 1 amp through the IRED and an exposure duration of over 1000 seconds, it is evident that there is no inherent danger in the implementation of this light source. In fact, the risk posed by the IRED under these conditions, even when viewing from a distance of 20 cm, which is the closest recommended measurement for realistic calculations, our case falls into the standardized exempt group (no hazard) established by OSRAM and the ICNIRP. The results of these calculations are depicted in figures A1 and A2, along with the resulting radiance from the IRED: 1.91E4 W/m/sr.

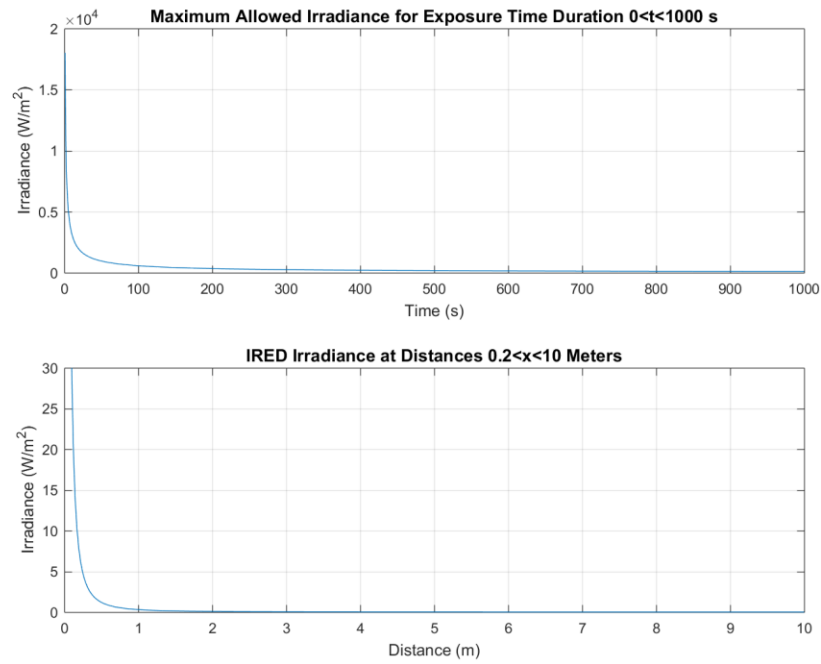


Figure 14. Comparison plots between the maximum allowed irradiance for a given time exposure, and the equivalent irradiance given by our infrared emitting diode, at the given distance for an exposure of 1000 seconds.

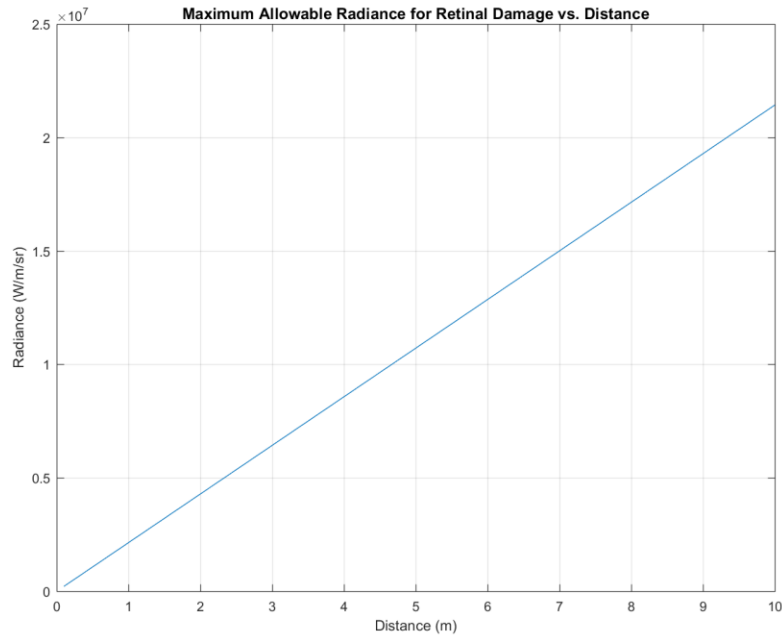


Figure 15. Maximum allowable radiance as a function of distance in $\text{W/m}^2/\text{sr}$. When analyzing the Radiance from our infrared light source ($1.91\text{E}4$ $\text{W/m}^2/\text{sr}$), it is clear that it is well below the danger threshold.

Appendix B: Function Tree

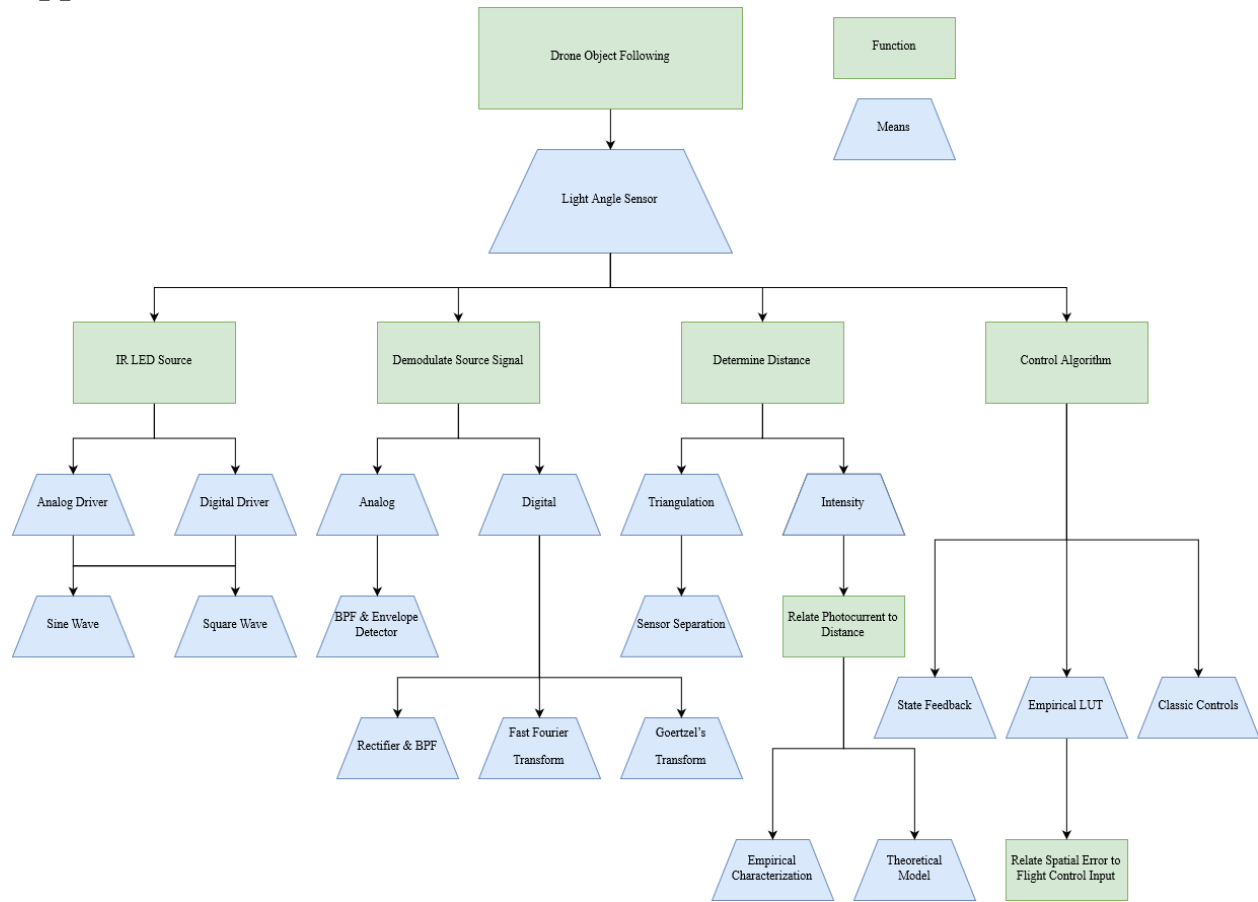


Figure 16. Function-Means Tree of major design choices and trade studies

Appendix C: Light Source Modulation Scheme

The overarching premise for modulating the light signal stems from the need to distinguish the IR light signal from any ambient IR light. Non-IR light is of minimal concern due to the tight wavelength response of the photodiode around 850nm. By modulating the light at a particular frequency, the signal received by the sensor can be analyzed at a particular frequency to reveal our signal of interest.

The first step in this was to choose a frequency that fit the parameters associated with avoiding ambient noise, as well as having the capability of being sampled by the microcontroller ADC. Therefore, we want to avoid frequencies like those present at 60 and 120 Hz in building lighting while also being low enough to be oversampled well above the Nyquist limit ($\gg 2 \cdot f_{\text{source}}$). We used these parameters to arrive at a source frequency of 500 Hz.

We proceeded to make a choice in signal shape between sine and square wave. The sine wave was initially appealing due to its distinguishing features of amplitude and phase however upon looking into the use of a square wave we found that it has many of the same attractive features. Sine waves are nice due to their spectral purity, but we confirmed that the majority of energy in a square wave is in the fundamental harmonic. When filtering for the given frequency the square wave can be discerned due to this quality and the sources features can be confirmed for tracking.

We chose the square wave and implemented it with a 555 timer initially; however, we looked into a digital option (Teensy LC) for modulating the signal, as well. We proceeded to test the two sources against each other and implement our chosen filter to determine how much of the fundamental energy was leaking out of our chosen 500 Hz bin. As shown in Figure 6, the digital solution has a greater magnitude at 500 Hz, exhibiting greater spectral purity and thus improved SNR.

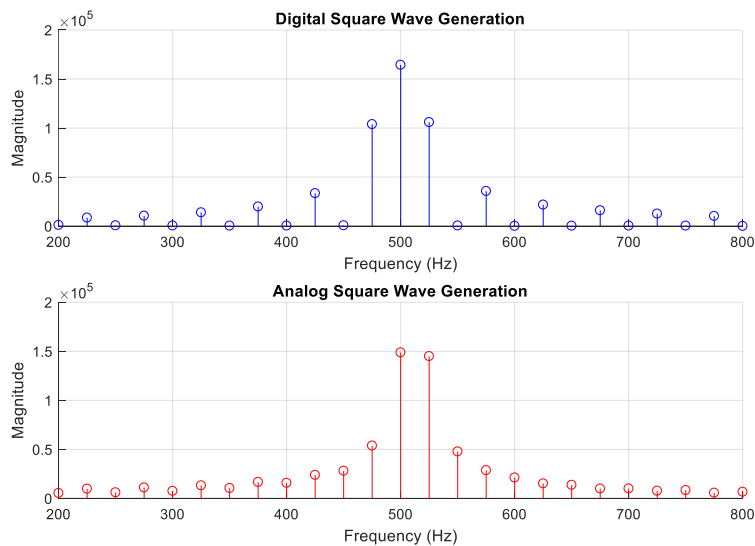


Figure 17. Detected Spectra of Analog and Digitally Generated Square Waves

An added feature of the digital solution using the Teensy LC returns to our overarching requirement that the system be replicable for future use by ADI. The removal of analog components allows for a more streamlined approach that increases performance across a range of our specifications. Analog components add a layer of complexity in achieving a consistent and precise solution and with this, the digital modulation approach emerges as the winner.

Appendix D: Processing Unit Selection

Another major decision within our solution space is the choice of processing unit that will sample the analog signals and perform the computation necessary for obtaining the three spatial coordinates of the light source. The first choice that must be made is that between an FPGA and a microcontroller. The predominant consideration dictating this choice is our objective to showcase the simplicity of the LAS in that its outputs are four analog signals, rather than a multitude of pixels in the case of a CMOS camera. In order to drive home the point that ADI's sensor requires a simpler interfacing system than the SOA, the choice of microcontroller over FPGA is beneficial. This is because programming an FPGA is generally a more complicated process than writing sequential code for a microcontroller. While not key requirements in creating our demonstration, cost and power consumption are typically key considerations for developers, both of which also point to the choice of a microcontroller. Lastly, an FPGA, since processing is parallelized, is more difficult to debug, which would slow our development process [20].

After deciding to use a microcontroller over FPGA for our data processing, a particular model of MCU still needs to be chosen. The sponsor had suggested two models: the STM Nucleo-64 development board as well as the ADICUP-360 development platform. Table 3 shows some relevant specifications of these two boards, as well as those of a third option: the Teensy 3.5.

Table 3. Processing MCU Comparison

	Teensy 3.5	STM Nucleo-64	ADICUP360
Physical Dimensions	6.2cm X 1.8cm	8.3cm X 7.0cm	10.2cm X 5.4cm
Clock Speed	120 MHz	82 MHz	16 MHz
ADC Sample Rate	4600 kSPS	2400 kSPS	3.9 kSPS
# ADCs	2	1	2
ADC Resolution	16 bits	12 bits	24 bits
Arduino Compatible	Yes	No	No
Price	\$24.25	\$12.74	\$45.00

[3, 8, 11]

Having chosen an IR modulation frequency of 500Hz, the system we choose must be capable of sampling the four analog signals at a rate high enough to capture our frequency of interest. We would like to sample the signal at several times its highest contained frequency for improved performance. The ADICUP360 platform can be ruled out just from this requirement. Even if both ADCs are used in tandem, the effective sampling rate that can be obtained is 6.8 kSPS. Split among the four channels, this implies we can sample each channel at a maximum of 1.7 kSPS, which is just over three times the highest frequency of interest. Particularly in a prototyping stage, it is in our best interest to choose a microcontroller that will not come close to limiting overall system performance. If, for some reason, we decide to increase our modulation frequency, the ADICUP360 platform would likely not be able to demodulate our signal.

We originally considered the Teensy 3.5 because some team members are familiar with it. We ultimately chose the Teensy platform for two main reasons: compatibility with the Arduino programming language and its small form factor. Arduino is a C-based embedded programming language that provides useful high-level functionality for frequently used processes. A microprocessor that is compatible with Arduino will speed up development of our prototype considerably. However, the level of abstraction provided by some Arduino functions come at a cost—speed. We decided that this would not be a major issue because the Teensy 3.5 boasts a 120MHz clock, partially mitigating the loss of speed in some Arduino functions. In addition, the Arduino functions can be overwritten in C or ARM Assembly for optimization if needed.

The Teensy's small form factor is another reason it would perform well in our application. With an area of only about 11 cm², the Teensy 3.5 development board could feasibly be placed directly on a small PCB that incorporates the entire sensor system. For these reasons, the Teensy 3.5 is our choice of processing unit in this project.

Appendix E: Flight Controller Selection

Having made a decision as to the means through which commands would be sent from the position controller to the flight controller (FC), a decision matrix can be designed to find a FC that would suit the project's needs.

Presented in table 4 are the options that were studied as potential flight controllers. A key requirement when picking the flight controller was the need for at least eight PWM inputs to the FC. Inputs I_0 through I_3 would provide user inputs from the handheld transmitter (throttle, yaw, roll, and pitch), along with input I_4 , which would serve as the mode select switch from the user. Inputs I_5 through I_7 would therefore become the position controller inputs for throttle, roll, and pitch.

Table 4. Flight Controller Comparison

Flight controller	PWM Inputs	Onboard Stability alg.	GUI ease of use	Customer support	Open Source	Cost
Pixhawk	None/1 PPM	Yes	2	3	Yes	\$204
Kiss FC	None/1 PPM	Yes	1	1	Yes	\$45
DJI A3	8	Yes	5	5	No	\$900
Parallax	8	Yes	4	4	Yes	\$149
Naza-M v2	8	Yes	5	5	No	\$159
Lum. Lux v2	None/1 PPM	Yes	4	4	yes	\$37

Appendix F: Analog Front End Design

The ADI LAS consists of four photodiodes. A photodiode is an optoelectronic device that outputs a photocurrent proportional to the intensity of incident light. Since “current” signals are cumbersome to process, our first task is to convert this current into a voltage with a circuit called a transimpedance amplifier.

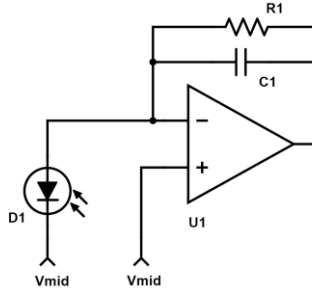


Figure 18. Compensated Transimpedance Amplifier Schematic

A transimpedance amplifier is implemented with an operational amplifier (op amp) in negative feedback. We selected an op amp (TLE2074) based on its extremely low input current noise rating (2.8 fA/√Hz) [7], which is critical in sensitive TIA applications. Below is a diagram of an op amp in negative feedback.

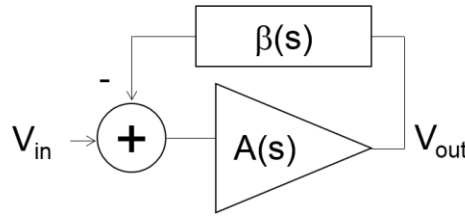


Figure 19. Operational Amplifier in Negative Feedback

We can see from the transfer function below that the system will become unstable (attempt to output an arbitrarily large voltage) when $A(s)\beta(s) = -1$.

$$\frac{V_{out}(s)}{V_{in}(s)} = \frac{A(s)}{1 + A(s)\beta(s)} \quad (6)$$

Thinking about this quantity in the complex plane, we can describe the unstable condition as $|A(s)\beta(s)| = 1$ and $\angle A(s)\beta(s) = -180$ degrees. Our goal is to prevent this condition from arising, namely by ensuring that the phase angle stays above -180 degrees when the quantity is at unity magnitude. This can be visualized in a frequency response with a quantity called the phase margin, which is the difference in the phase response from -180 degrees when the magnitude response reaches 0dB (unity gain).

We can avoid the occurrence of this condition by adding a zero to the system in the form of a feedback capacitor. After adding the feedback capacitor, the transfer function becomes:

$$(s)\beta(s) = \frac{A_0(1 + sRC_F)}{(1 + s\tau)(1 + sR(C_F + C_p))} \quad (7)$$

[13]

Where A_0 is the open-loop gain of the op amp, τ is a parameter that can be calculated from the open-loop gain and gain-bandwidth product, C_F and C_p are the feedback capacitance and parasitic capacitance of the photodiode, and R is the feedback resistance.

We also need to ensure that we have sufficient gain of our photocurrent and that our frequency of interest (modulation frequency) is not being attenuated. The relationship between the photocurrent and TIA output voltage is given by the following:

$$\frac{V_{out}}{I_{light}} = \frac{R}{(1 + sRC_F)} \quad (8)$$

Since the photocurrent generated by each photodiode is on the order of micro amps, we would need to apply a gain on the order of 1 million to bring the signal into the volt range. For this reason, a $2M\Omega$ feedback resistor and a $15pF$ feedback capacitor was chosen. To verify that this design would satisfy our objective of stability, sufficient gain, and a passband that extends beyond our modulation frequency, both equation 7 and 8 were simulated in MATLAB. Plots can be viewed in figures 20 and 21

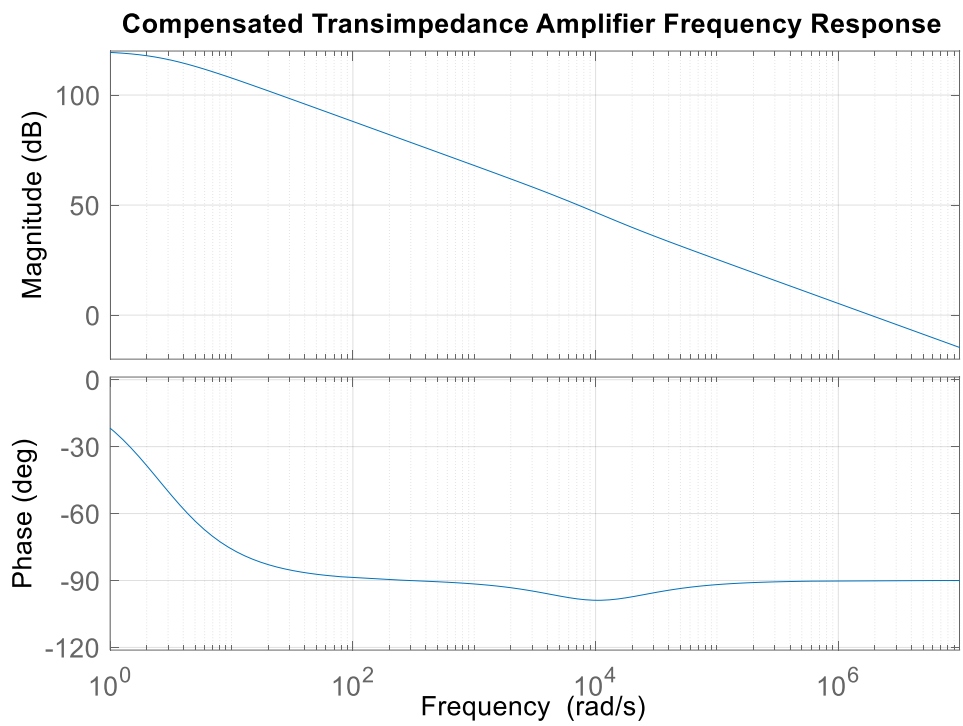


Figure 20. Compensated TIA Frequency Response

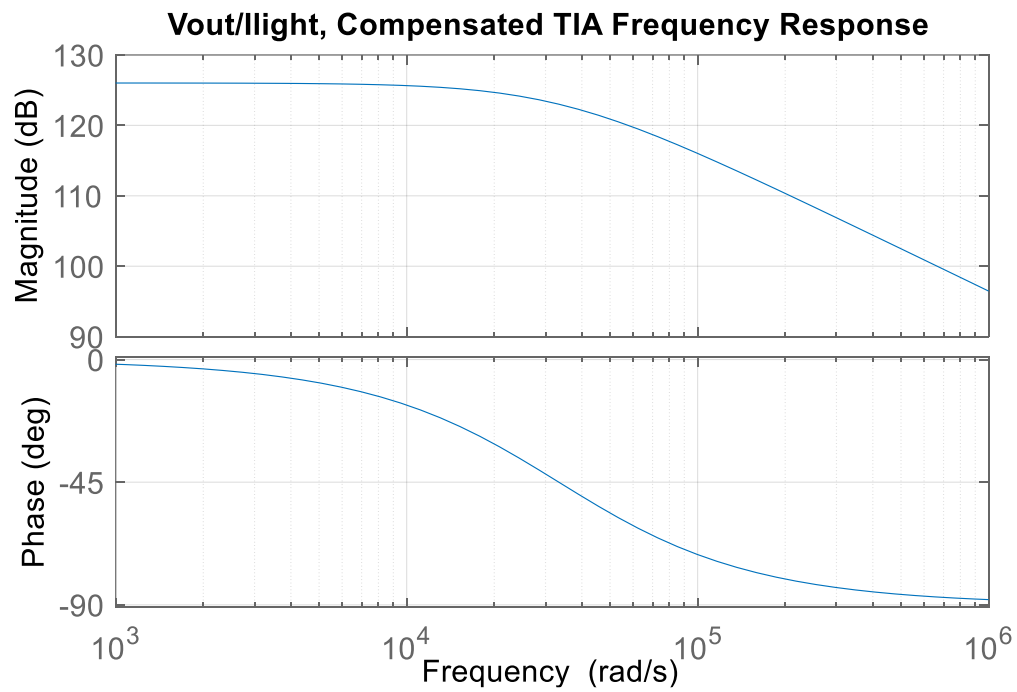


Figure 21. V_{out}/I_{light} TIA Frequency Response

The major takeaways are that with our chosen values of feedback resistor and capacitor, we achieve stability (89.8 degree phase margin), appropriate passband location, and sufficient passband gain (126dB).

Now that a voltage proportional to the photodiode current response has been obtained, the signal must be sampled and processed. However, one crucial piece of analog circuitry must be incorporated prior to sampling—the anti-aliasing filter (AAF). To understand the need for the AAF, we can think of the sampling process as multiplying our time-domain signal by a comb function (a series of Dirac delta functions). Now thinking in the frequency domain, the spectrum of the sampled signal can be represented as the Fourier transform of the time-domain signal convolved with the Fourier transform of the Comb function (as a result of the convolution theorem). Since the Fourier transform of a comb function is another comb function, the resulting spectrum is a periodic replication of the original signal's spectrum. If the original signal has significant spectral content above half the sampling frequency, spectral overlap (also called aliasing) will occur. To avoid this, an anti-aliasing low-pass filter was implemented with a cutoff frequency close to our signal of interest. Since our sampling rate is several times larger than our modulated light frequency, a first-order passive filter was deemed sufficient, since such a filter with cutoff at about 500Hz would have -20dB attenuation at 5000Hz (half of the 10 kHz sampling rate). Going forward, our team will experiment with a higher-order AAF and compare performance. The AAF currently being implemented is shown in Figure 22.

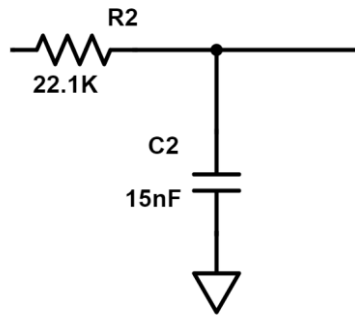


Figure 22. Schematic representation of AAF

These designs were replicated identically for each of the four photodiode channels.

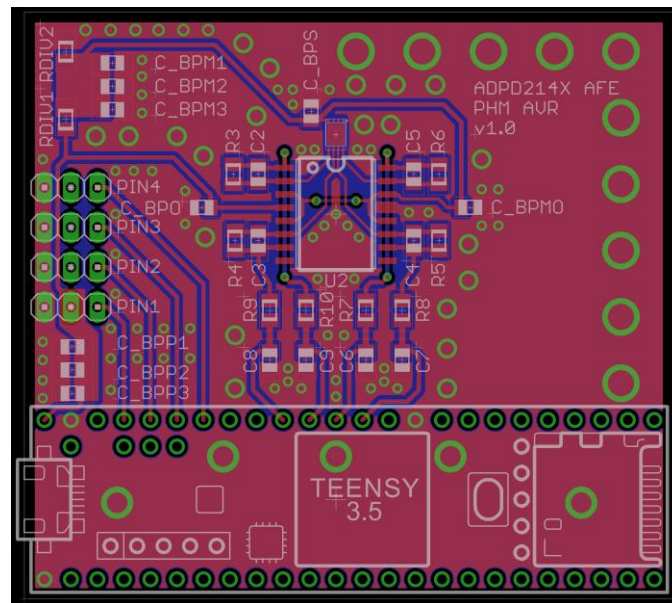


Figure 23. Printed Circuit Board Layout for Sensor AFE & MCU

Our sensor AFE has reached the level at which we are confident in its functionality and can scale it in size and accuracy by using SMD components on a PCB. With this, the PCB has been designed and sent out for fabrication.

There are many considerations to be made when laying out the PCB as its functionality can be affected by a multitude of factors and parasitic effects. The aspects considered have included:

Inductance Loops: As signals complete their loops to their respective components they create a magnetic field based on the parasitic inductance associated with loop length. This can create noise on the board that can interfere with other signals and decrease SNR. This is ameliorated by reducing loop lengths, shielding sensitive signals, and using bypass capacitors.

Signal Coupling: Signals can couple with one another through magnetic fields and with this, it is important to note which signals are sensitive to noise and take steps to limit it. The way that this has been limited is by noting that our 4 channel signals from the sensor are sensitive all the way to their output so they have been separated by a ground signal between each to cause magnetic fields to be limited to the signals interaction with this ground.

High frequency noise: Due to the fact that the MCU must take in the sensor signals after the AAF's it has been placed on the same board to limit the distance these signal must travel. With this, the HF functions of the MCU produce noise that can also interfere with the signals. To deal with this we have placed ground planes on the top and bottom that prevent this noise from wanting to couple with our 4 channel signals.

Reference Consistency: Each signal is passing through various components and at the same time its magnitude is being referenced to the ground that particular component utilizes. It is worth acknowledging that grounds meaning can vary throughout locations on the board so efforts must be made to keep signal referencing consistent. This has been approached by placing bypass capacitors for components as well as their ground references as close together as possible.

Future steps for PCB work will include validating this design's functionality and making any alterations that may be required in a future version as well as designing a PCB for the LED driving circuit.

Appendix H: Benchtop Test Setup

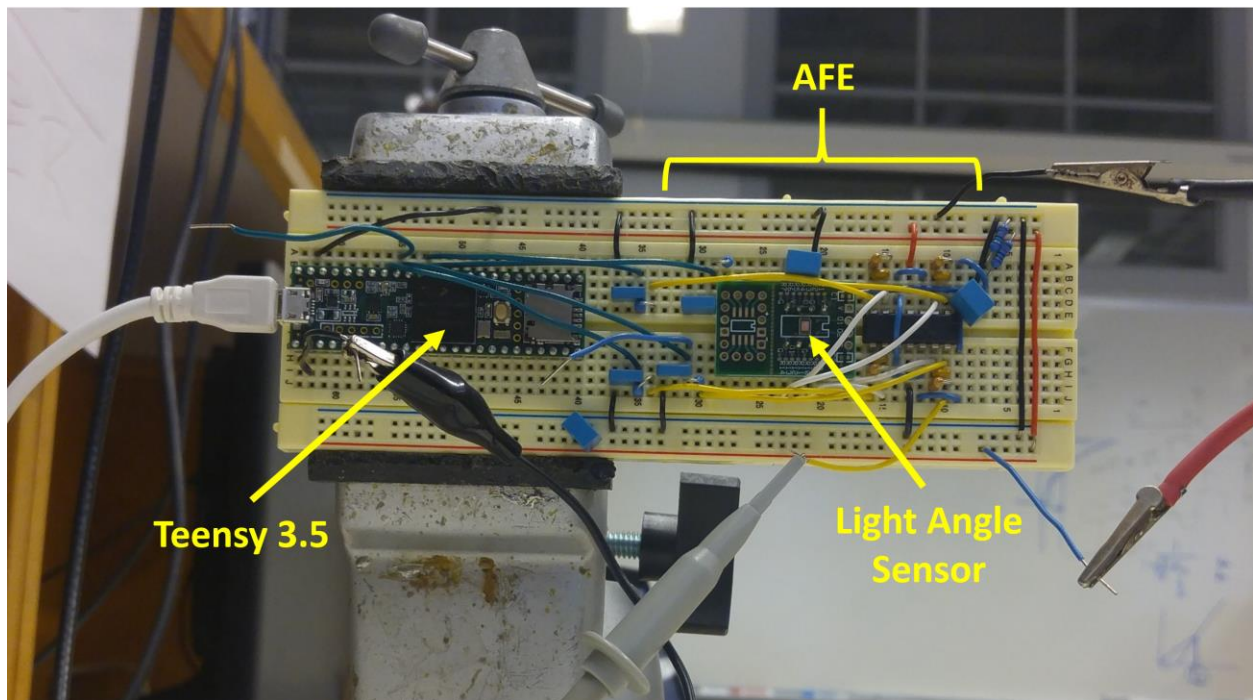


Figure 24. Image of Sensor System Circuitry in Benchtop Setup

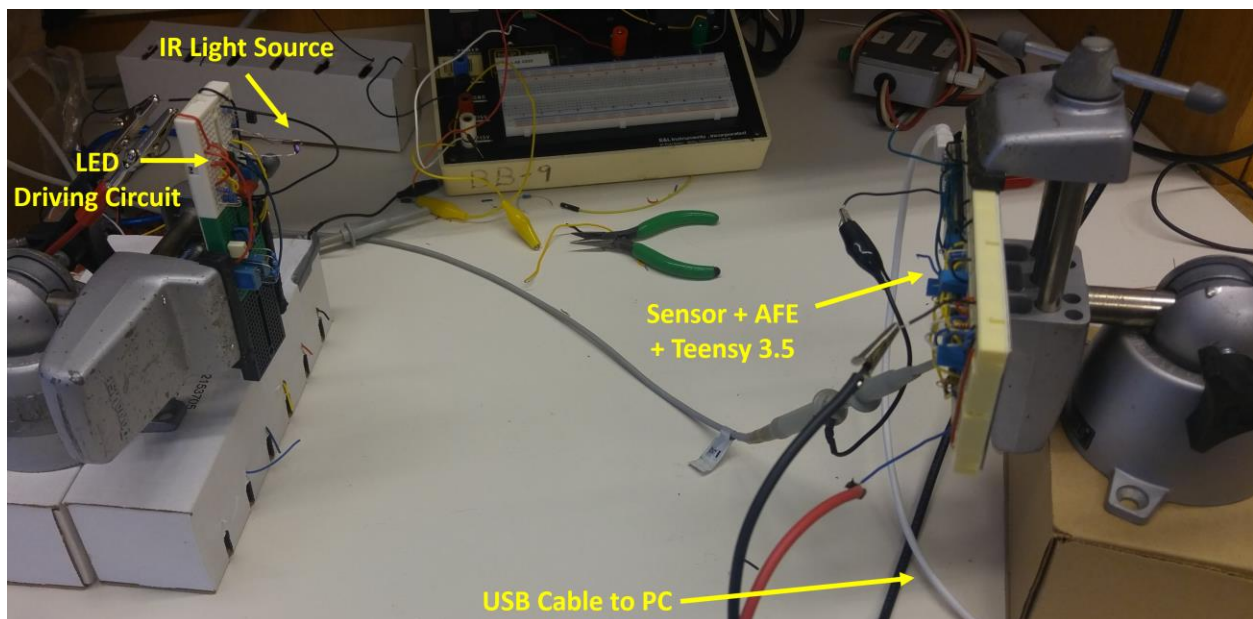


Figure 25. Image of Benchtop Setup, Light Source and Sensor System

Appendix I: Teensy Code

```
#include <TimerOne.h>
#include <math.h>
#include "Plotter.h"

#define modFreq 500 //LED modulation frequency
#define Fsample 10000 //per channel sampling rate (Hz)

#define XR 2
#define XL 3
#define YB 5
#define YT 4

#define XR_index 0
#define XL_index 1
#define YB_index 2
#define YT_index 3

const float targetFreq = 500;

const int samplesPerPeriod = Fsample / modFreq;
const int NPeriods = 10; //number of periods to capture in one sampling burst
const int N = NPeriods*samplesPerPeriod; //how many samples to take before processing them

int dataBuffer[4][200]; //buffer for storing data\

int dataBufferIndex = 0;

float sine;
float cosine;
float Q1;
float Q2;
float coeff;

float XRmag = 0;
float XLmag = 0;
float YBmag = 0;
float YTmag = 0;
float X = 0;
float Y = 0;
float intensity = 0;

int Navg = 5;
int avgBuffer[5];
float alpha = 0.9;
float Yvalue = 0;
float Xvalue = 0;

Plotter p;

void setup() {

    pinMode(XR, INPUT);
    pinMode(XL, INPUT);
    pinMode(YB, INPUT);
```

```

    pinMode(YT, INPUT);

    pinMode(6, OUTPUT);
    analogReadResolution(16);
    analogReference(0);
    Timer1.initialize(1e6 / Fsample);
    Timer1.attachInterrupt(samplingISR);

    initGoertzel(targetFreq);

    p.Begin();
    p.AddXYGraph("XY Position Plot", 100, "X Axis", X, "Y Axis", Y);
}

void samplingISR() {
    if (dataBufferIndex < N) {
        dataBuffer[XR_index][dataBufferIndex] = analogRead(XR);
        dataBuffer[XL_index][dataBufferIndex] = analogRead(XL);
        dataBuffer[YB_index][dataBufferIndex] = analogRead(YB);
        dataBuffer[YT_index][dataBufferIndex] = analogRead(YT);
        dataBufferIndex++;
    }
}

void resetGoertzel() {
    Q1 = 0;
    Q2 = 0;
}

void initGoertzel(float targetFreq) {
    int k;
    float floatN = (float)N;
    float w;

    k = (int)(0.5 + ((floatN * targetFreq) / Fsample));
    w = (2.0*PI*k) / floatN;
    sine = sin(w);
    cosine = cos(w);
    coeff = 2.0 * cosine;

    resetGoertzel();
}

float performGoertzel(uint8_t channel_index) {

    Q1 = 0;
    Q2 = 0;

    int sum = 0;
    int mean = 0;
    for (int i = 0; i < N; i++) {
        sum = sum + dataBuffer[channel_index][i];
    }

    mean = (int)(sum / N);
}

```



```

    for (int i = 0; i < N; i++) {
        float Q0;
        Q0 = (coeff * Q1) - Q2 + (float)dataBuffer[channel_index][i] - mean;
        Q2 = Q1;
        Q1 = Q0;
    }
    return (Q1*Q1 + Q2*Q2 - (Q1*Q2*coeff));
}

void loop() {

    if (dataBufferIndex > (N - 1)) {

        noInterrupts();
        digitalWrite(6, HIGH); //for timing
        XRmag = performGoertzel(XL_index);
        XLmag = performGoertzel(XR_index);
        YBmag = performGoertzel(YB_index);
        YTmag = performGoertzel(YT_index);
        digitalWrite(6, LOW); //for timing
        X = ((XRmag - XLmag) / (XRmag + XLmag));
        Y = (YTmag - YBmag) / (YTmag + YBmag);
        p.Plot();
        interrupts();
        dataBufferIndex = 0;
    }
}

```

Appendix J: Histogram of Acquired Data

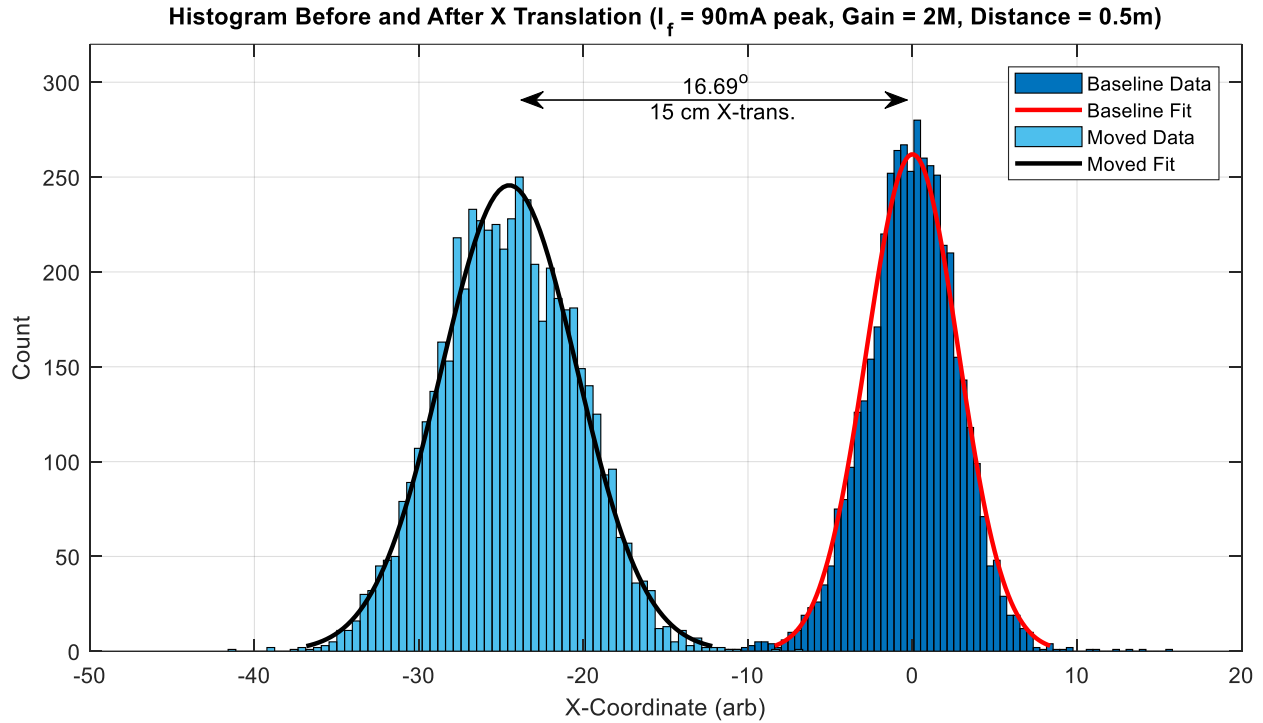


Figure 26. Histogram of X Measurement Before and After Translation

Figure 26 shows the distribution of X measurement data before and after translating the light source in the X direction by 15cm at a distance of half a meter. A translation of 15cm is equivalent to a 16.7 degree angle change at this distance. As expected, the SNR decreased slightly after translation due to a slightly farther distance from the sensor. The important takeaway is that the means of two roughly Gaussian distributions are clearly very different. After implementing a moving average filter and increasing the LED intensity, the measurements will likely be very reliable.

Appendix K: Total Costs

Table 5. Total Costs

	Item	Quantity	Price
Sensor-Related Components	EMITTER IR 860NM 1.5A 3SMD	2	2 x \$4.46
	EMITTER IR 860NM 1A SMD	2	2 x \$4.96
	EMITTER IR 860NM 100MA RADIAL	2	2 x \$0.56
	LED INFRARED SMD	2	2 x \$4.07
	SOT23 TO DIP ADAPTER	1	\$0.95
	SOT23 TO DIP ADAPTER	4	4 x \$0.94
	SNAPS 9V 6" LEADS I-STYLE HD	1	\$0.68
	BATTERY ALKALINE 9V	1	\$1.88
	SHIPPING CHARGES APPLIED	1	\$7.50
	TRANS NPN 60V 5A TO-126	5	5 x \$0.61
	SHIPPING CHARGES APPLIED	1	\$7.50
	PCB Fabrication	3	\$54.20
	SHIPPING CHARGES APPLIED	1	\$5.00
Sensor-Related Component Subtotal			\$221.97
Drone-Related Components	Lumenier 3300mAh 3s 35c Lipo Battery	2	2 x \$34.99
	Multicopter Propeller With DJI Fitting DJI Style 10x4.5 Black (CW) (4pcs)	2	2 x \$4.24
	Multicopter Propeller DJI Style 10x4.5 Orange (CCW) (4pcs)	2	2 x \$3.68
	Multistar Propeller With DJI Fitting 10x4.5 Black (CW) (2pcs)	2	2 x \$2.79
	Multistar Propeller With DJI Fitting 10x4.5 Black (CCW) (2pcs)	2	2 x \$2.79
	Twisted 10CM Female To Female Servo Lead (JR) 22AWG (10pcs/Set)	1	\$1.89
	SHIPPING CHARGES APPLIED	1	\$8.97
	Multicopter Propeller DJI Style 10x4.5 Orange (CCW) (4pcs)	1	\$3.68
	Multicopter Propeller With DJI Fitting DJI Style 10x4.5 Black (CW) (4pcs)	1	\$4.24
	S500 Glass Fiber Quadcopter Spare Landing Gear Leg (Black) (4pcs)	2	2 x \$2.53
	SHIPPING CHARGES APPLIED	1	\$7.93
	ELEV-8 Flight Controller	1	\$149.00
	SHIPPING CHARGES APPLIED	1	\$29.96
Drone-Related Component Subtotal			\$307.71
TOTAL			\$529.68

Appendix L: Future Plans

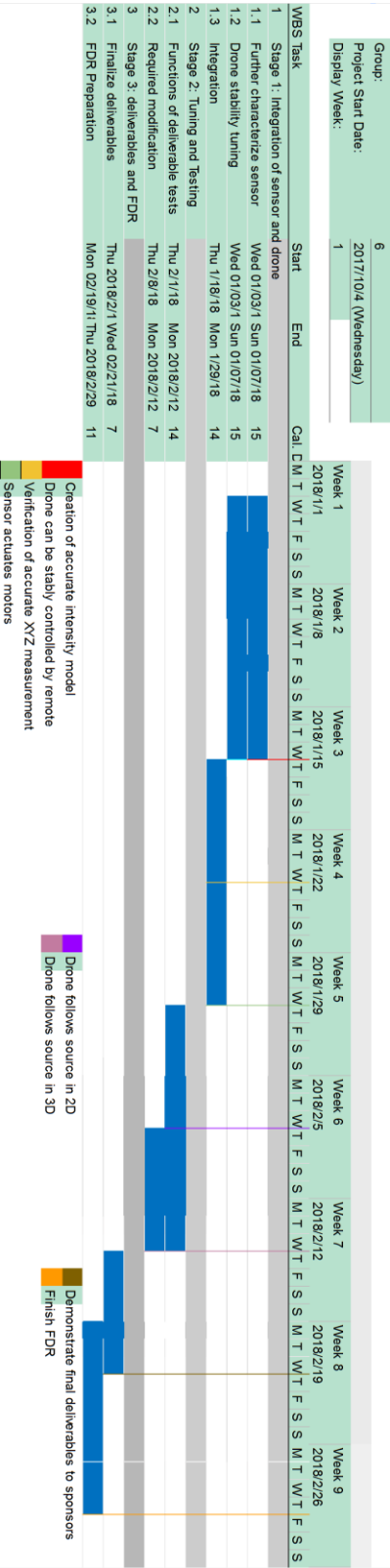


Figure 27. Winter term Gantt chart

Appendix M: Revised Client Agreement

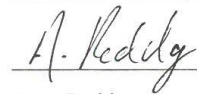
Agreement of Expectations (Revised for Preliminary Design Review)

ENG 89/90: Drone Object Sensing with Light Angle Sensor

Our group agrees to deliver the following completed items by the end of ENG 90:

- A printed circuit board (PCB) that incorporates the light angle sensor, analog front-end circuitry and digital signal processing necessary to measure X, Y, and Z position of an asynchronous light source
- A PCB that implements a square-wave LED driving circuit which will serve as the IR light source in the demonstration
- A functioning demonstration that showcases the operability of the light angle sensor in a drone-based object-following application
- Appropriate documentation of hardware and software implementation details

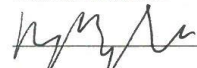
ENG 89/90 Group:



Arun Reddy



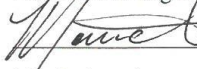
Hamza Alsarhan



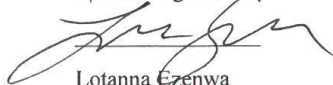
Ping-Jung Lju



Prescott McLaughlin



Martin Anguita



Lotanna Ezenwa

Sponsors:



Tyler Ray



Dvij Bajpai